International Journal of Nanomedicine

Dovepress

open access to scientific and medical research

Open Access Full Text Article

ORIGINAL RESEARCH

Pioglitazone-Loaded Cartilage-Targeted Nanomicelles (Pio@C-HA-DOs) for Osteoarthritis Treatment

Junyan Chen[1,2,*], Wuyan Xu[2,*], Tianming Dai[3,*], Songsong Jiao[2], Xiang Xue[2], Jiayang Jiang[1,2], Siming Li[1,3], Qingqi Meng[3]

[1]Guizhou Medical University, Guiyang, 550025, People's Republic of China; [2]Department of Orthopaedics, Guangzhou Red Cross Hospital of Jinan University, Guangzhou, 510220, People's Republic of China; [3]Guangzhou Institute of Traumatic Surgery, Guangzhou Red Cross Hospital of Jinan University, Guangzhou, 510220, People's Republic of China

*These authors contributed equally to this work

Correspondence: Siming Li; Qingqi Meng, Guangzhou Institute of Traumatic Surgery, Guangzhou Red Cross Hospital of Jinan University, Guangzhou, 510220, People's Republic of China, Tel +8613929526981, Email drsmli@163.com; mengqingqi@jnu.edu.cn

Background: Hyaluronic acid (HA) is a popular biological material for osteoarthritis (OA) treatment. Pioglitazone, a PPAR-γ agonist, has been found to inhibit OA, but its use is limited because achieving the desired local drug concentration after administration is challenging.

Purpose: Herein, we constructed HA-based cartilage-targeted nanomicelles (C-HA-DOs) to deliver pioglitazone in a sustained manner and evaluated their efficacy in vitro and in vivo.

Methods: C-HA-DOs were chemically synthesized with HA and the WYRGRL peptide and dodecylamine. The products were characterized by FT-IR, ^{1}H NMR, zeta potential and TEM. The drug loading rate and cumulative, sustained drug release from Pio@C-HA-DOs were determined, and their biocompatibility and effect on oxidative stress in chondrocytes were evaluated. The uptake of C-HA-DOs by chondrocytes and their effect on OA-related genes were examined in vitro. The nanomicelle distribution in the joint cavity was observed by in vivo small animal fluorescence imaging (IVIS). The therapeutic effects of C-HA-DOs and Pio@C-HA-DOs in OA rats were analysed histologically.

Results: The C-HA-DOs had a particle size of 198.4±2.431 nm, a surface charge of −8.290±0.308 mV, and a critical micelle concentration of 25.66 mg/Land were stable in solution. The cumulative drug release from the Pio@C-HA-DOs was approximately 40% at pH 7.4 over 24 hours and approximately 50% at pH 6.4 over 4 hours. Chondrocytes rapidly take up C-HA-DOs, and the uptake efficiency is higher under oxidative stress. In chondrocytes, C-HA-DOs, and Pio@C-HA-DOs inhibited H_2O_2-induced death, reduced intracellular ROS levels, and restored the mitochondrial membrane potential. The IVIS images confirmed that the micelles target cartilage. Pio@C-HA-DOs reduced the degradation of collagen II and proteoglycans by inhibiting the expression of MMP and ADAMTS, ultimately delaying OA progression in vitro and in vivo.

Conclusion: Herein, C-HA-DOs provided targeted drug delivery to articular cartilage and improved the role of pioglitazone in the treatment of OA.

Keywords: nanoparticles, micelles, drug delivery, hyaluronic acid, knee joint

Introduction

Osteoarthritis (OA) is a refractory, degenerative and complex disease. Due to its various sequelae and complex symptoms, OA places a great economic burden on patients and local health systems. From the perspective of epidemiology, the OA more prevalent women and elderly individuals.[1,2] The most common site of OA is the knee joint, followed by the hip joint and hand joint.[3] Evidence suggests that obesity, trauma, and genetic factors are inextricably linked to the occurrence and development of OA.[4,5] Obesity not only has a metabolic effect on OA due

Received: 4 July 2023
Accepted: 7 October 2023
Published: 18 October 2023

to the resulting higher levels of inflammatory factors, but also increases the burden on the knee and hip joint, leading to chronic mechanical damage, which leads to further OA development. Strenuous exercise, accidents and surgical injuries can also contribute to the pathology of OA.[6]

Currently, OA management involves surgical and pharmacological interventions, with nonsteroidal anti-inflammatory drugs (NSAIDs) and corticosteroids being the mainstay of clinical pharmacotherapy.[7] However, NSAIDs cause clear adverse reactions, involving the gastrointestinal tract and cardiovascular and cerebrovascular aspects. The long-term use of steroids can also lead to osteoporosis, hypertension, diabetes, and a series of diseases. In addition, when the abovementioned drugs are taken orally, higher doses are required to achieve effective blood drug concentrations due to drug clearance by the liver and plasma, which further aggravates the resulting adverse reactions.[8] Thus, intra-articular injection has been the preferred route of drug administration for OA treatment. However, some problems with frequent injections, such as the risk of infection, cost and pain, still need to be overcome.[9]

To surmount the limitations of the above treatment methods, it is imperative to explore novel drug delivery approaches that achieve higher local drug concentrations with lower systemic doses, which would lead to enhanced therapeutic efficacy and reduced adverse reactions. Nanodrug delivery technology has been widely used for this purpose, including some nanomaterials with high permeability, specificity, and long-term retention in vivo and in vitro.[10–12] Extensive evidence has shown that nanomaterials can be used as drug delivery systems to bind to target tissues and deliver drugs directly and specifically. In addition, previous studies have confirmed that the nanomaterials themselves can have a variety of biological functions, such as changing cell behaviour, providing antitumor, anti-inflammatory, and immunomodulatory effects, and promoting tissue repair.[13–19]

Pioglitazone, a classic antihyperglycemic agent, exerts its therapeutic effects by selectively activating peroxisome proliferator-activated receptor gamma (PPAR-γ), one of the three subtypes of this receptor. PPAR-γ is highly expressed in the liver, skeletal muscle, kidney, heart, vascular walls, and articular cartilage. Studies have shown that hyperglycaemia downregulates the expression of PPAR-γ in human and murine chondrocytes, leading to the induction of inflammation and cartilage degradation caused by IL-6 and matrix metalloproteinase (MMP)-13.[20] As a PPAR-γ agonist, pioglitazone can reverse the increases in the levels of inflammatory factors that result from the accumulation of advanced glycation end products in vivo, restore the suppressed AMPK and SIRT-1 signalling pathways, and inhibit OA.[21–24] Furthermore, pioglitazone has been found to exhibit anti-inflammatory effects by inhibiting the NF-κB signalling pathway.[25] Studies have also demonstrated that pioglitazone can maintain chondrocyte vitality by activating cellular autophagy.[26]

Hyaluronic acid (HA), a repeating unit disaccharide, is one material that has been used to develop structures for the treatment of OA through tissue engineering. The average molecular weight and distribution of HA vary depending on its source, which in turn determines its physicochemical properties, such as degradation and hardness of the HA-derived tissue-engineered constructs. HA is present in both synovial fluid and the extracellular matrix of articular cartilage and demonstrating various therapeutic effects in the treatment of OA, as extensively discussed in numerous reviews.[27,28] The most significant role of HA lies in its physicochemical effects in joint lubrication, which has led to the development of various HA-based injectable therapies aimed at restoring the diminished viscoelasticity of synovial fluid. Compared to other biopolymers, HA possesses inherent biological advantages as it is a major component of synovial fluid and the extracellular matrix of chondrocytes. Recently developed HA-based tissue engineering approaches have primarily focused on improving the biocompatibility and intrinsic biological and physical properties of HA.[29]

The WYRGRL peptide is a short, 6 amino acid peptides discovered after affinity and biological screening of bovine cartilage tissue. It binds to collagen type II, in a sequence-specific manner and shows long-term retention in cartilage tissue when modified with poloxamer.[30] The WYRGRL peptide can directly bind to dexamethasone covalently, which enhances the depth of dexamethasone delivery to cartilage and significantly reduces the level of inflammatory markers.[31] This modification strategy also plays a role in the design of other cartilage-targeted nanoparticles.[32] For nanoparticles with negative surface charges, modification with the WYRGRL peptide led to 50% retention in mouse knee cartilage after 24 hours, which was twice that of nontargeted nanoparticles.[27] In a 1,4,7,10-tetraazacyclododecane-1,4,7,10-tetraacetic acid amide(DOTAM) drug delivery platform, the DOTAM drug-loaded platform combined with the WYRGRL peptide was better retained in cartilage than the unmodified platform with the same surface charge, which

indicates that the peptide can affect both the early stage and late stage of OA in the term of the loss of glycosaminoglycan.[33]

Based on the aforementioned information, the aim of this study is to develop a novel approach using HA-based nanomicelles surface modified with cartilage-targeting peptides to enable targeted delivery of the encapsulated PPAR-γ agonist pioglitazone to cartilage. The administration of these nanomicelles via intra-articular injection is expected to achieve a therapeutic effect by slowing the progression of OA.

Materials and Methods

Materials

HA (Mw=5 kDa) was purchased from Freda Biopharmaceutics Co., Ltd. (Shandong, China). 4-(4,6-Dimethoxy-1,3,5-triazin-2-yl)-4-methylmorpholinium chloride (DMTMM), tetrahydrofuran (THF), dodecylamine, pyrene, hydrochloric acid, and methanol were purchased from Aladdin Biochemical Technology Co., Ltd. (Shanghai, China). Pioglitazone was purchased from Sigma (St. Louis, MO, USA). The lipid-soluble dye Cy5 was purchased from Lablead Biotechnology Co., Ltd. (Beijing, China). The WYRGRL peptide was synthesized by IGE Biotechnology Ltd. (Guangzhou, Guangdong, China). The CCK-8 assay kit, JC-1 assay kit, Hoechst 33,258 reagent, TRIzol reagent and penicillin–streptomycin solution were purchased from Beyotime Biotechnology Co., Ltd. (Shanghai, China). PrimeScript RT Master Mix and TB Green RT-PCR reagent were purchased from Takara Bio Inc. (Beijing, China). The primer sequences were obtained from Sangon Biotech (Shanghai) Co., Ltd. (Shanghai. China). PBS, DMEM/F12 medium, 0.25% trypsin, and foetal bovine serum were purchased from Gibco (California, USA). Collagen type II, Aggrecan, MMP-13, and disintegrin-like and metalloproteinase with thrombospondin motifs (ADAMTS)-4 antibodies were purchased from Proteintech (Wuhan, China).

Preparation and Structural Characterization of the Cartilage-Targeted HA Nanomicelles (C-HA-DOs)

The grafting of hydrophobic groups onto HA was conducted following the procedure described in the literature (Figure 1).[34] Sodium hyaluronate (400 mg, 5 kDa) was dissolved in 30 mL of deionized water, and the pH of the solution was adjusted to 6.0 with 0.01 mol/L HCl solution. Then, 1 mmol of DMTMM was added, and the reaction mixture was stirred at 600 r/min in an ice bath for 2 hours to fully activate the carboxyl groups of HA. Subsequently, a solution containing 185 mg of dodecylamine in 30 mL of THF was slowly added dropwise with stirring, and the reaction temperature was raised to room temperature. The reaction was carried out in a sealed reactor with stirring at 600 r/min for 24 hours. The products were dialyzed against 80%, 60%, 40% and 20% ethanol solutions for 24 hours to

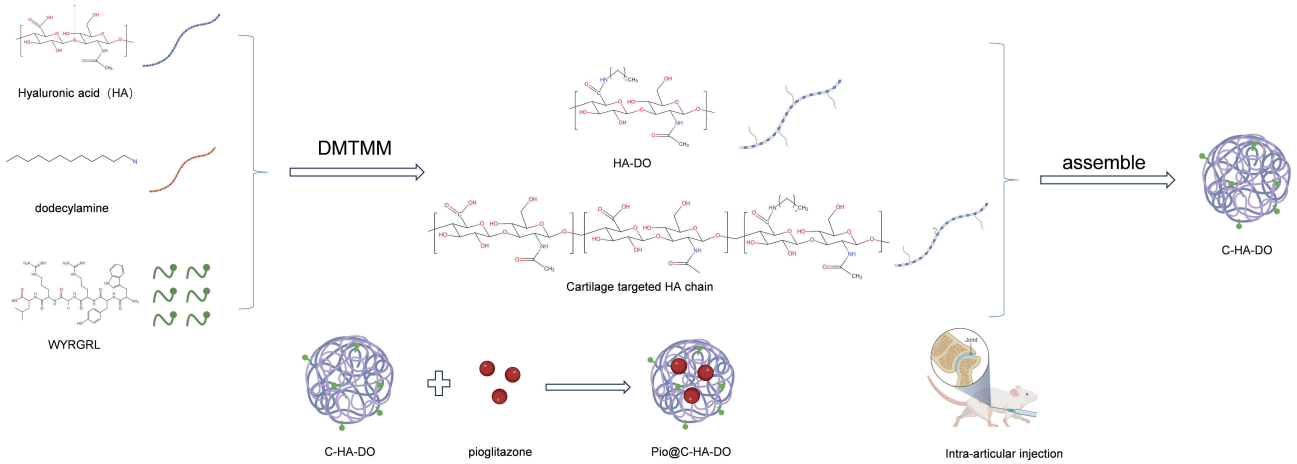

Figure 1 Synthesis of Pio@C-HA-DO.
Abbreviations: DMTMM, 4-(4,6-dimethoxy-1,3,5-triazin-2-yl)-4-methylmorpholinium chloride; HA, hyaluronic acid; HA-DO, hyaluronic acid nano micelles; C-HA-DO, cartilage-targeted hyaluronic acid nano micelles; Pio@C-HA-DO, cartilage-targeted hyaluronic acid nano micelles load with pioglitazone.

remove unreacted dodecylamine and THF and then dialyzed against deionized water for 48 hours. The volume of dialysate was 2 L each time, and the dialysate was changed every 2 hours. After dialysis, hydrophobic group-grafted HA micelles were obtained by freeze drying and named HA-DOs.

Following the same procedure, 400 mg of HA was dissolved in 30 mL of deionized water, and 0.5 mmol of DMTMM was added. The mixture was stirred at 600 r/min in an ice bath for 2 hours to activate the carboxyl groups of HA. Separately, 400 mg of the WYRGRL peptide was dissolved in 30 mL of deionized water, and 92.5 mg of dodecylamine was dissolved in 20 mL of THF. These two solutions were slowly added dropwise to the activated HA solution with stirring at room temperature under sealed conditions, and the reaction was allowed to proceed for 24 hours. The resulting mixture was then subjected to dialysis against ethanol solutions under the same conditions as those described above for 24 hours. Subsequently, dialysis was continued using deionized water for 48 hours to completely remove any unreacted and self-crosslinked WYRGRL peptide. Finally, the dialysis solution was freeze dried to obtain cartilage-targeted HA chains.

The cartilage-targeted HA chains and HA micelles were mixed in equal proportions in water. The mixture was subjected to 30 minutes of ultrasonication to achieve homogeneity. After sufficient stabilization, the mixture was filtered through a 0.22 μm microporous membrane and freeze dried for preservation. This process resulted in the formation of C-HA-DOs.

The structural characterization and comparison of HA and C-HA-DOs was then conducted. The solid powders of both samples were mixed with KBr powder, thoroughly ground, and then dried in an infrared drying oven. Subsequently, the samples were pressed into pellets and analysed using Fourier transform infrared (FT-IR) spectroscopy (Thermo Fisher Scientific Nicolet iS5, USA). The obtained infrared spectra were analysed and compared. To analyse the raw HA, HA-DOs, and C-HA-DOs, each sample was dissolved in D_2O, and one-dimensional proton spectra were acquired by nuclear magnetic resonance spectroscopy (^{1}H NMR, 400 MHz, Bruker, Germany) in the peak range of 0–9 ppm. The proton peaks in the obtained ^{1}H NMR spectra were analysed to calculate the grafting efficiency of dodecylamine and qualitatively examine the binding of the WYRGRL peptide.

Critical Micelle Concentration (CMC) of the C-HA-DOs

The CMC of the C-HA-DOs was determined using the traditional pyrene fluorescence probe method. A certain volume of pyrene solution in methanol was added to each test tube, and the methanol was evaporated in a dark room to form a thin film of pyrene at the bottom of the tube. C-HA-DO solutions with different concentration ranging from 3.0×10^{-3} mg/L to 0.1 mg/L were added to each test tube, resulting in a final pyrene concentration of 6.0×10^{-7} mol/L. The solutions were sonicated for 30 minutes and left in a dark room at 4°C overnight. The fluorescence intensity of pyrene in the test tubes was measured using a fluorescence spectrophotometer. The excitation wavelength was set to 334 nm, and the emission wavelength was set to 350–450 nm. The excitation and emission slit widths were both 2.5 nm. The fluorescence intensity at 373 nm was recorded as I1, and the fluorescence intensity at 384 nm was recorded as I3. A data plot was generated by plotting the logarithm of the C-HA-DO concentration on the x-axis and the ratio of the two fluorescence intensities (I1/I3) on the y-axis. The concentration at which the I1/I3 ratio was highest was identified, and semilogarithmic linear regression models were fitted to the data. The CMC value was calculated based on the regression model with the highest fitting degree. By employing this pyrene fluorescence probe method and analysing the fluorescence intensity data, the CMC of the C-HA-DOs was accurately determined, providing valuable information about the self-assembly behaviour and stability of the micellar system.

Particle Size, Zeta Potential and Morphological Observations of the C-HA-DOs

According to the determined CMC value, an appropriate amount of C-HA-DOs was dissolved in PBS solutions with pH values of 7.4 and 6.4. The solutions were then subjected to 30 minutes of ultrasonication to ensure uniform dispersion of the micellar particles. These prepared micellar solutions were used for the experimental measurements, while the remaining solutions were stored at 4°C. Two C-HA-DOs sample solutions at a concentration of 0.5 g/L were placed in 2 mL cuvettes. The particle size and surface zeta potential of the C-HA-DOs were analysed at room temperature using

a Zetasizer (Malvern, Zetasizer Nano ZS90). The corresponding polydispersity index (PDI) was also recorded. Each sample was measured at least 3 times.

An appropriate amount of C-HA-DOs was weighed and dissolved in deionized water to prepare a solution with a concentration of 5×10^{-4} mg/L. Then, 10 μL of the prepared solution was drop-cast onto a copper grid covered with a carbon support membrane. After a few minutes of incubation, the excess liquid was removed using filter paper. Subsequently, 2% phosphotungstic acid staining solution was added, and after 1–2 minutes of staining, the excess negative stain was removed using filter paper. The sample was then dried and observed by transmission electron microscopy (TEM, FEI Tecnai 12).

Stability of the C-HA-DOs

We measured the particle size of the C-HA-DOs in solutions with different pH values as a function of time by dynamic light scattering (DLS). To simulate the pH values of normal joint fluid, mild osteoarthritic synovial fluid, and severe osteoarthritic synovial fluid, PBS solutions with pH values of 7.4, 7.0, and 6.4 were prepared. C-HA-DOs solutions were prepared at each pH with a concentration of 5×10^{-4} mg/L and subjected to 30 minutes of ultrasonication at 37°C. Subsequently, 2 mL of the micellar solutions at pH 7.4 and 7.0 were transferred to a cuvette for size analysis using Zetasizer. Three replicates were performed for each sample, and the remaining prepared solutions were stored in a constant temperature incubator (37°C, 5% CO_2). Every 24 hours, 2 mL of each solution was collected for size analysis; this process was repeated for a total of 6 days. The collected data were recorded and processed for analysis.

Establishment of an Absorbance-Pioglitazone Concentration Standard Curve

The standard curve of pioglitazone can be established by ultraviolet spectrophotometry.[35] In this experiment, UV–visible spectrophotometry was used to establish the linear relationship between absorbance and the concentration of pioglitazone in 0.1 mol/L HCl. The specific operating procedure was as follows.

Pioglitazone powder was weighed and dissolved in 0.1 mol/L HCl at room temperature. This solution was diluted with HCl to generate solutions with concentrations of 0.01, 0.02, 0.04, 0.06, 0.08, 0.1, 0.2, and 0.4 g/L, and these solutions were thoroughly mixed. The absorbance of each solution was measured using a UV–Vis spectrophotometer (Thermo Fisher Evolution 350) with 0.1 mol/L HCl solution as the background. The absorbance at 269 nm was measured more than three times for each solution concentration. The measured data were summarized, and a linear regression model was established.

In the linear model recovery test, three solutions with known concentrations of pioglitazone hydrochloride were prepared (0.05, 0.1, and 0.2 g/L). The absorbance of each solution was measured, and these results were converted to concentrations with the previously established linear model and compared with the theoretical concentration. From these data, the recovery rate and relative standard deviation were calculated.

Preparation and Drug Loading of Pio@C-HA-DOs

Pioglitazone drug-loaded micelles (Pio@C-HA-DOs) were prepared by dialysis.[33] One hundred milligrams of C-HA-DOs were weighed and dissolved in 100 mL of PBS to make micelle solution A, and 40 mg of pioglitazone was weighed and dissolved in 10 mL of DMSO solution to make drug solution B. An appropriate amount of solution A was added to an appropriate amount of solution B to obtain a certain ratio (Table 1). The drug fully entered the micelles under continuous agitation. A 100 Da dialysis bag filled with deionized water was used for 24 hours of dialysis to

Table 1 Composition of the Drug-Loaded Micelles

Drug Proportion in Pio@C-HA-DOs (w/w)	1:2	1:2.5	1:5	1:10	1:25
Solution A (mL)	0.8	0.9	0.95	0.975	0.99
Solution B (mL)	0.2	0.1	0.05	0.025	0.01

Notes: Solution A, 1 g/L C-HA-DOs in PBS; solution B, 4 g/L pioglitazone in DMSO.

simultaneously block the drug pioglitazone and remove DMSO so that the drug could further enter the hydrophobic core of the micelles. Finally, the Pio@C-HA-DOs were separated from the free pioglitazone by ultrafiltration, and the Pio@C-HA-DOs product was collected and lyophilized for storage.

The ultrafiltrate obtained during the preparation of the drug-loaded micelles was adjusted to a concentration of 0.1 mol/L with HCl and mixed by random mixing. The absorption rate of free pioglitazone was measured by ultraviolet spectrophotometry at 269 nm, and the drug concentration of pioglitazone was calculated by comparison with the established pioglitazone standard curve. The calculation formulas are as follows:

$$\text{Encapsulation efficiency (EE)} = \frac{W_0 - W_F}{W_0} \times 100\% \tag{1.1}$$

$$\text{Drug loading (DL)} = \frac{W_0 - W_F}{W_0 + W_{C-HA-DO}} \times 100\% \tag{1.2}$$

Where W_0 and $W_{C\text{-}HA\text{-}DO}$ represent the mass of pioglitazone and C-HA-DOs infused during preparation, respectively, and W_F represents the mass of free pioglitazone in the ultrafiltrate.

Drug Release from the Pio@C-HA-DOs

The in vitro drug release from Pio@C-HA-DOs was determined by dialysis.[36] The specific procedure was as follows. First, the desired formulation of drug-loaded micelles was added to PBS solutions with pH values of 7.4 and 6.4 at a final drug-loaded micelle concentration of 1 g/L. Then, the dialysis bag was placed in a 50 mL centrifuge tube, and 50 mL of PBS solution was added to the tube. The tube was placed on a shaker in a constant temperature incubator (37°C, 5% CO_2). At 1, 2, 4, 8, 12, 24, 48, 72, and 96 hours, a 100 μL sample of the release medium was taken and placed in an EP tube, and the same volume of the corresponding pH PBS solution was added to maintain a constant volume overall. The 100 μL sample was lyophilized, resuspended, and centrifuged in 10 μL of 0.1 mol/L HCl solution, and then the concentration of the drug was determined. Each time point utilized 3 replicates. The cumulative release of pioglitazone at each time point was calculated as follows:

$$E_X\,(\%) = \frac{V_m \sum_1^{x-1} C_i + V_o C_x}{m_o} \times 100\% \tag{1.3}$$

Where V_0 represents the volume of release medium (50 mL), m_0 represents the total amount of drug encapsulated, V_m represents the volume of each sample, C_x and E_X represent the sampling concentration and cumulative release rate at the Xth sampling point, and C_i represents the drug concentration of the ith detection point before n times.

In vitro Experiments

Extraction, Cultivation, and Treatment of Primary Chondrocytes from SD Rats

All SD rats were purchased from Guangdong Medical Laboratory Animal Centre, and all animal-related experiments were approved by the Animal Care and Use Committee of Guangzhou Red Cross Hospital, Guangdong Province, China (approval No. 2021–191-01), and conducted in strict accordance with the guidelines for Ethical Review of Laboratory Animal Welfare in China (GB/T35892-2018). Primary (P0) chondrocytes were isolated from the knee joints of 4-week-old SD rats and cultured in DMEM/F12 complete medium (with 10% foetal bovine serum), 100 IU/mL penicillin G and 100 μg/mL streptomycin. After digestion with trypsin, P0 chondrocytes were passaged, and P2 chondrocytes were used for subsequent experiments.

Cytocompatibility Testing and Other in vitro Cellular Activity Experiments with C-HA-DOs

P2 chondrocytes were digested and seeded into 96-well plates at a density of 5000 cells per well. After the cells had completely attached to the wall, the medium was removed, DMEM/F12 complete medium with C-HA-DOs at concentrations of 0.05, 0.1, 0.2, 0.5, 1, 2, or 5 g/L was added, and the cells were cultured again in a constant temperature incubator. After 24 and 48 hours, the medium was replaced by DMEM/F12 basal medium containing 10% CCK-8

solution. After incubated for 2 hours, the absorbance value (OD value) at 450 nm was measured by a microplate reader, and the final obtained data were plotted and analysed.

The H_2O_2-induced chondrocyte injury model was established as follows. First, P2 chondrocytes were seeded in 96-well plates at a density of 5000 cells per well. After the cells had completely attached, the medium was removed and replaced with 100 μL of complete medium containing 100, 200, 300, 400, 500, 600, 700, or 800 μmol/L H_2O_2 for incubation in a constant temperature incubator (37°C, 5% CO_2) for 24 hours. After washed with PBS, DMEM/F12 basal medium containing 10% CCK-8 was added for incubation in a constant temperature incubator (37°C, 5% CO_2). Two hours later, the OD value at 450 nm was measured by a microplate reader.

According to the above experimental results, an appropriate concentration of H_2O_2 was selected, and P2 chondrocytes were seeded in 96-well plates following the same protocol. The cells were treated with 400 μmol/L H_2O_2 or H_2O_2 in combination with 0.1, 0.3, or 1 g/L HA, or synthetic C-HA-DOs. The culture plate was incubated in an incubator (37°C, 5% CO_2) for 24 hours, the cell activity was detected by a CCK-8 kit as described above, and the OD value was detected.

Effects of C-HA-DOs and Pio@C-HA-DOs on Oxidative Stress in Chondrocytes

This experiment consisted of four groups: blank control (Group C), H_2O_2-induced model (Group R), H_2O_2-induced model treated with C-HA-DO (H_2O_2+C-HA-DO, Group P1), and H_2O_2-induced model treated with Pio@C-HA-DO (H_2O_2+Pio@C-HA-DO, Group P2). Chondrocytes were seeded in a 12-well plate using the same method as described earlier. After the cells had attached, the cells were treated with 400 μmol/L H_2O_2 alone or in combination with 1 g/L C-HA-DOs or Pio@C-HA-DOs. After 24 hours of incubation in a constant temperature incubator, the level of reactive (ROS) and mitochondrial membrane potential in the chondrocytes were evaluated by a ROS kit and JC-1 kit according to the manufacturer's protocol.

C-HA-DOs Cellular Uptake

C-HA-DOs uptake experiments by chondrocyte determined to methods from other studies.[37] First, lipid-soluble Cy5-labeled C-HA-DOs (Cy5-C-HA-DOs), were generated by dissolving Cy5 in DMSO at a concentration of 0.2 mg/mL. Then, 10 mg of C-HA-DOs was dispersed by ultrasonication into 10 mL of PBS, 200 μL of Cy5 solution was added, and the mixture was stirred in a dark chamber overnight to obtain Cy5-C-HA-DOs. Chondrocytes with and without oxidative stress were incubated with Cy5-C-HA-DOs for 1 and 4 hours, washed 3 times with PBS and fixed with 4% paraformaldehyde for 15 minutes. After an additional 3 washes with PBS, the nucleus was stained with a Hoechst kit. The distribution of Cy5-C-HA-DOs in chondrocytes was observed by fluorescence microscope, and statistical analysis was performed.

Quantitative Real-Time qPCR

The effects of ROS, HA, C-HA-DOs and Pio@C-HA-DOs on the expression levels of OA-related genes and CD44 were detected by real-time PCR. The specific methods were as follows. Total RNA was extracted from treated chondrocytes from each group using TRIzol. Then, RNA was reverse transcribed with a PrimeScript RT Master Mix kit, and the obtained cDNA was subjected to RT–qPCR with TB Green RT–PCR reagent. Each sample had three replicate wells. mRNA expression was normalized to that of GAPDH using the 2-ΔΔCT method. The primer sequences are listed in Table S1 (The primer sequence).

In vivo Experiments

Animal Model Groupings and Surgical Induction of OA in Model Rats

Male SD rats (n=3/group) aged 8 weeks (and weighing approximately 180 g) were randomly divided into 4 groups: the sham operation control (Group C), destabilization of the medial meniscus (DMM) model (Group R), DMM model treated with intra-articular injection of C-HA-DOs (DMM+C-HA-DO, Group P1), and DMM model treated with intra-articular injection of Pio@C-HA-DOs (DMM+Pio@C-HA-DO, Group P2). The specific operation by which the meniscus instability model was established was described in other studies.[38] Starting from the first week after the operation, SD rats were removed from their cages and exercised on a small animal running wheel for 2 hours every day to promote exercise and aggravate wear of the knee joint.

Groups P1 and P2 were injected with 50 μL of C-HA-DO solution and Pio@C-HA-DOs solution, respectively, each at a concentration of 1 g/L, and Group C and Group R were injected with the same dose of normal saline. Injections were performed once every 4 days. The tibial plateau of the right knee of each rat was taken for observation and pathological histological analysis, and the OARSI score of histopathology was determined based on the relevant literature.[39]

In vivo Imaging System (IVIS) Experiment

To generate indocyanine green (ICG)-labelled C-HA-DOs (ICG-C-HA-DOs), ICG was first dissolved in deionized water to prepare a 1 g/L solution. Blank C-HA-DOs were also used to generate 10 mL of a 1 g/L solution. The two solutions were mixed, homogenized by ultrasonication for 30 minutes, and magnetically stirred at 600 r/min overnight in a dark room. ICG-labelled micelles (ICG@C-HA-DOs) at a concentration of 1 g/L were obtained by performing dialysis and lyophilization in the same way as described earlier and stored at 4°C in a dark room. On days 7, 5, 3, 2, and 1 before observation, 50 μL of ICG@C-HA-DO solution and free ICG were injected into the right knee cavity with a micro syringe to ensure that no fluid leaked out into the joint cavity. Ketamine was used during observation. The rats were anaesthetized with a mixture of ketamine and xylazine (1:2). After the animals were anaesthetized, they were placed in the dark box of the small animal in vivo imaging system (FX Pro). The position of the rats was adjusted to ensure that the right knee joint of each rat was imaged. The excitation wavelength was 760 nm, and the emission wavelength was 830 nm.

Statistical Analysis

The data are presented as the mean values ± standard deviations. Statistical significance was determined using two-way analysis of variance. Graphs and figures were generated using GraphPad Prism software. The FT-IR spectroscopy results were analysed using OMNIC software. NMR spectra were analysed using MestReNova 14 software. Fluorescence images and immunohistochemical images were processed and statistically analysed using ImageJ software. The in vivo fluorescence images of the animals were processed and analysed using Buker MI SE software. For the reported data, the symbol "*" denotes $P < 0.05$, "**" denotes $P < 0.01$, and "ns" indicates no statistically significant difference. All statistically analysed data included a minimum of 3 samples.

Results and Discussion

Synthesis and Characterization of the C-HA-DOs

DMTMM was used as the catalyst for the synthesis of the chondrocyte-targeting HA micelles with WYRGRL peptide modification due to its good stability in aqueous solution.[40] The structure of the HA micelles was characterized by FT-IR (Figure 2a). First, the carbonyl peak at 1616 cm^{-1} from the HA raw material was weakened, and peaks at 1649 cm^{-1} and 1566 cm^{-1} appeared, which are characteristic of amide bonds (amide-I and amide-II, respectively). Both peaks are related to the vibration of the nitrogen in the amide bond. The peaks appearing at 2854 cm^{-1} and 2924 cm^{-1} were due to C-H vibrations and correspond to -CH2- and -CH3, respectively; HA itself does not contain long-chain alkanes. After comparison of the data, it was determined that dodecylamine and HA had successfully coupled.

The reaction was further characterized by ^{1}H NMR spectroscopy (Figure 2b–d). The HA micelles showed new signals at 0.85 ppm and 1.23 ppm without HA, a methyl signal at 0.85 ppm and a methylene signal at 1.23 ppm. By comparing the integration of the end-matrix subpeak of HA with the two emerging peaks, the grafting rate of dodecylamine was determined to be 25.25%, which guarantees that one carboxyl group within every four HA repeat units was successfully replaced with a lipophilic chain. A tryptophan peak between 7–8 ppm was observed in the C-HA-DOs sample, with a small peak at 0.85 ppm. This indicates that the WYRGRL peptide was partially grafted onto the C-HA-DOs.

Characterization of the C-HA-DOs

The CMC is an important structural property of surfactants. It represents the minimum concentration of micelles in solvent at which active molecules can form colloidal aggregates, and the micelles that form under these conditions can self-assemble. Pyrene is a commonly used hydrophobic probe with very low solubility in water. The fluorescence intensity of pyrene in methanol solution can be measured with a fluorescence spectrophotometer at an excitation

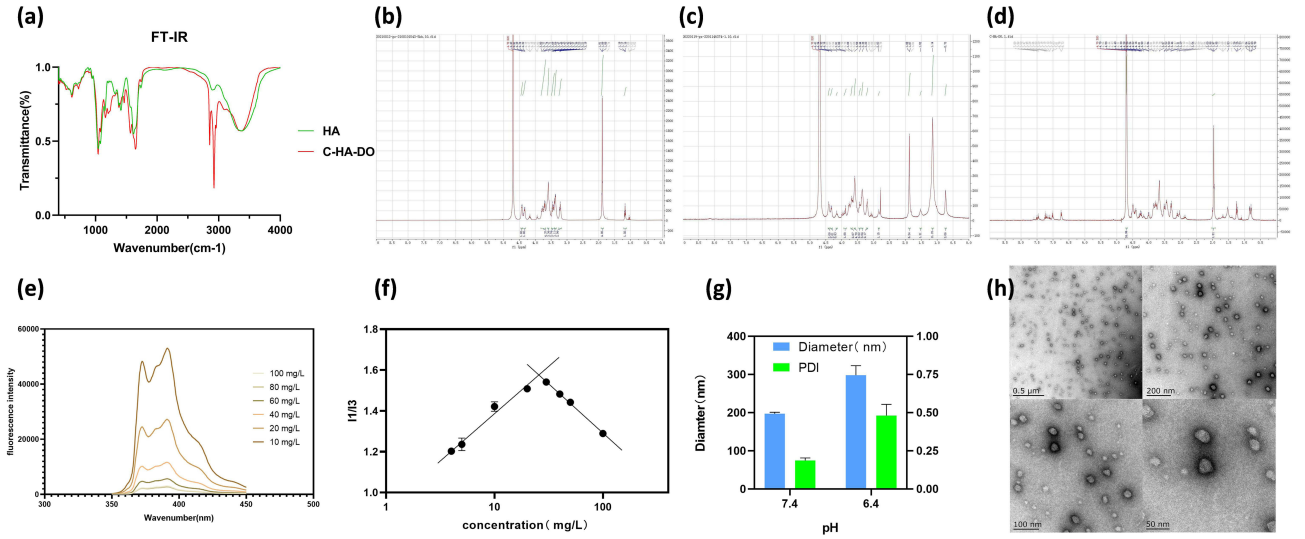

Figure 2 Characterization of C-HA-DOs. (**a**) FT-IR spectra of HA and C-HA-DOs. ^{1}H NMR spectra of HA (**b**), HA-Dos (**c**) and C-HA-Dos (**d**) (ppm, in D_2O). (**e**) Fluorescence intensity of pyrene (in methanol). (**f**) CMC of C-HA-DOs. (**g**) Particle size and PDI of C-HA-DO in solutions with different pH values. (**h**) TEM images of C-HA-DOs (0.5 g/L,0.5 μm-50 nm).

Abbreviations: HA, hyaluronic acid; HA-DO, hyaluronic acid nano micelles; C-HA-DO, cartilage-targeted hyaluronic acid nano micelles; FT-IR, Fourier transform Infrared; ^{1}H NMR, hydrogen nuclear magnetic resonance spectroscopy; CMC, critical micelle concentration. PDI, polydispersity index; TEM, transmission electron microscope.

wavelength of 334 nm. The spectrum of pyrene in methanol showed multiple fluctuating peaks in the detected wavelength range (Figure 2e). The ratio of the fluorescence intensity of the first peak (I1) at 373 nm and the third peak (I3) at 384 nm (I1/I3) is linearly correlated to the logarithm of the concentration of pyrene in the solvent. As the micelle concentration in solution increased, the increase in the intensity of the third peak of pyrene in solution caused an alteration in the I1/I3 ratio, and the concentration at this point was taken as the first CMC. The CMC value of the C-HA-DOs was the intersection of two fitted linear models and was calculated to be 25.66 mg/L (Figure 2f). The lower CMC is the concentration at which C-HA-DOs can assemble into spherical micelles in aqueous solution at a lower concentration to encapsulate the drug. After the micelle solution is injected into the joint cavity, the volume of the solution increases, and the micelle solution is diluted. However, the micelles can still maintain their spherical shape, which is conducive to the stability of C-HA-DOs in the joint cavity.

DLS is a physical characterization method that is often used to detect the particle size distribution of particulate matter in solutions and suspensions. The particle sizes measured by DLS in the two different solutions were different (Figure 2g). In PBS at pH 7.4, which simulated the physiological synovial fluid microenvironment, the particle size of C-HA-DOs was smaller and the PDI was also smaller. However, in pH 6.4 PBS, the C-HA-DOs' particle size increased, and two peaks formed. The micelles became larger in the acidified joint synovial fluid (pH 6.4). According to analysis of the figure, the particle size in the pH 7.4 environment was (198.4±2.431) nm, while the particle size in the pH 6.4 PBS environment was (298.3±16.305) nm. Thus, a lower pH resulted in larger particles. Moreover, the PDI greatly increased under acidic conditions, indicating that the structure of the C-HA-DOs changed with pH, which facilitates drug release from the inner hydrophobic core of the micelles in the arthritic environment.

The measured zeta potential values were also recorded during the experiment (Table 2). Since HA itself is an acidic mucopolysaccharide, the surface charge of HA became positive after modification with the cartilage-targeting peptide WYRGRL. The surface charge of the C-HA-DOs in pH 7.4 PBS was only −8.290±0.308 mV, while in pH 6.4 solution, the zeta potential of the C-HA-DOs rose to −0.9380±0.374 mV, which was close to electronic neutrality. The gap between the collagen network and glycosaminoglycan chains in the cartilage matrix layer is 100–200 nm, and the micellar particles prepared in this experiment are close to 200 nm in size.[41] Moreover, a less negative surface charge reduces the charge barrier for the electrostatic exclusion of micellar particles. Therefore, the C-HA-DOs can successfully penetrate the surface of the cartilage layer and enter the deep layer of the cartilage matrix.

Table 2 Particle Sizes and Zeta Potentials of the C-HA-DOs

	pH 7.4	pH 6.4
Diameter (nm)	198.4±2.431	298.3±16.305
Zeta potential (mV)	−8.290±0.308	−0.9380±0.374

Notes: Data are expressed as the mean ± standard deviation (n=3).

The morphology of the C-HA-DOs was characterized using TEM (Figure 2h). After negative staining, the micellar particles showed a slightly irregular circular shape with a particle size of approximately 37 nm, which was much smaller than the particle size measured by DLS. After drying on the copper net, the hydrogen bonds between the hydrophilic groups of the micelle and water are destroyed, resulting in the overall contraction of the micelle shell.

Stability of the C-HA-DOs

The stability of the micelle particles in solution was also reflected by the change in particle size detected by DLS (Figure 3a). At the first time point, the particle size of the C-HA-DOs increased with decreasing pH at 37°C; this was also true at room temperature. The results showed that the C-HA-DOs could maintain a small particle size (less than 0.5 μm) after 72 hours in PBS at pH 7.4, and then the particle size gradually increased with time. The corresponding change trend

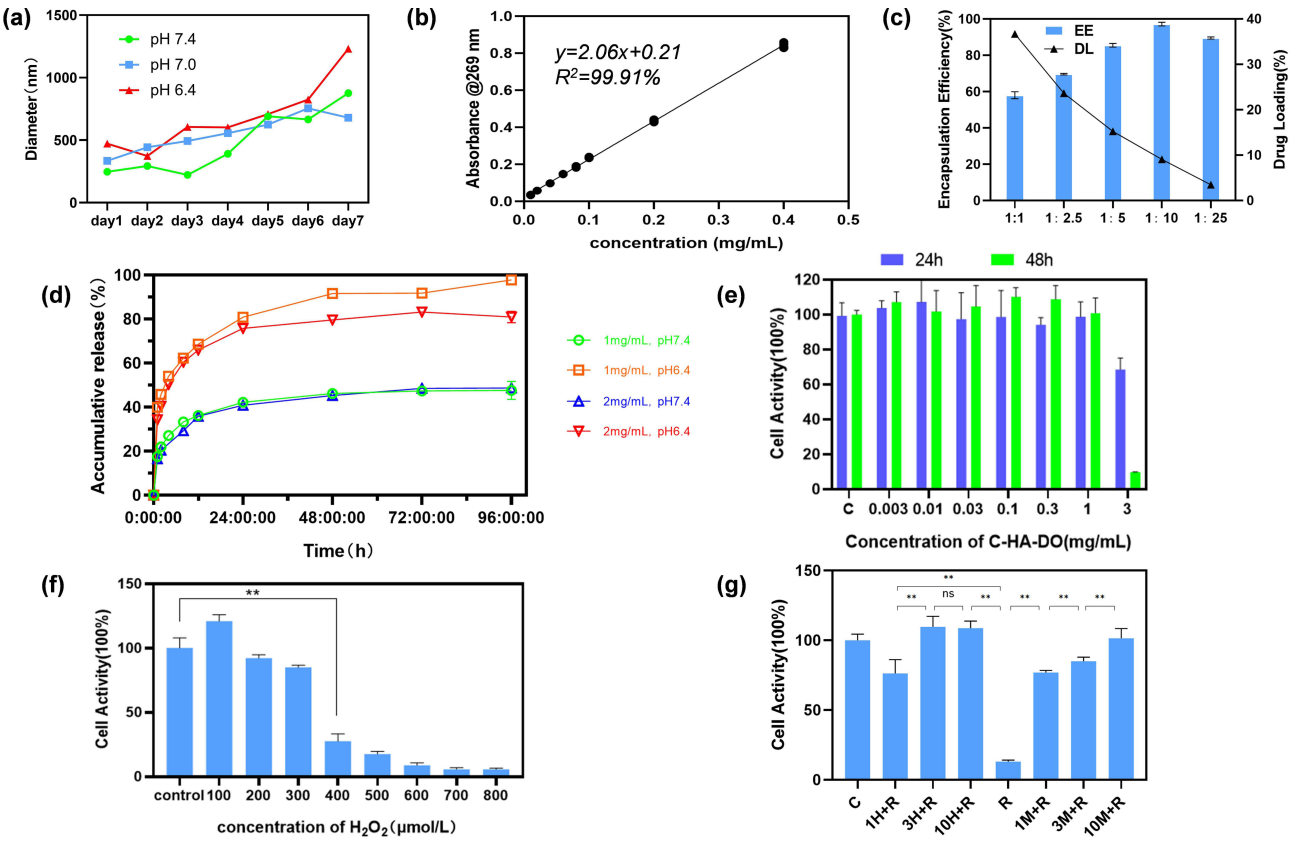

Figure 3 Characterization of Pio@C-HA-DO and CCK-8 result. (**a**) Stability of C-HA-DOs in PBS solutions with different pH values (pH=7.4, 7.0, and 6.4). (**b**) Standard curve of pioglitazone in 0.1 mol/L HCl (absorption peak:269 nm). (**c**) Encapsulation efficiency and drug loading rate of C-HA-DOs (n≥3). (**d**) Cumulative drug release from Pio@C-HA-DOs (37°C, PBS, n=3). (**e**) Cytocompatibility of C-HA-DOs at 24 and 48 hours. (**f**) Effects of H_2O_2 chondrocyte viability. (**g**) HA and C-HA-DOs inhibit chondrocyte death induced by H_2O_2 (n≥3).

Notes: *P<0.05, **P<0.01, ns, not significant.

Abbreviations: EE, encapsulation efficiency; DL, drug loading; C-HA-DO, cartilage-targeted hyaluronic acid nano micelles. HA, hyaluronic acid; HA-DO, hyaluronic acid nano micelles; C-HA-DO, cartilage-targeted hyaluronic acid nano micelles; 1H, 0.1 g/L hyaluronic acid; 3H, 0.3 g/L hyaluronic acid; 10H, 1 g/L hyaluronic acid; 1M, 0.1 g/L cartilage-targeted hyaluronic acid nano micelles; 3M, 0.3 g/L cartilage-targeted hyaluronic acid nano micelles; 10M, 1 g/L cartilage-targeted hyaluronic acid nano micelles; R, 400 μmol/L H_2O_2.

in particle size was also observed in the solutions with different pH values. The difference in the size range of the micellar particles in solution indicates that the stability of these micellar particles varies in different environments; C-HA-DOs in solution with lower pH values are more unstable and their size changes early. The micelles remained stable for approximately 72 hours in only the simulated synovial fluid environment. This would allow the micellar particles in human synovial fluid to not undergo dramatic morphological changes, reducing their deformation and avoiding drug burst release under the influence of deformation, while the changes in the other two environments allow rapid drug release in the synovial fluid or cartilage matrix layer in OA. The temperature for the C-HA-DO stability test was 37°C. Notably, the particle size of the C-HA-DOs was previously tested at room temperature, and the results of the two tests are significantly different. The particle size at 37°C is generally larger than that in the same solution at room temperature, indicating that the temperature of the micelle solution may also affect the micelle particle size and stability.

Pio@C-HA-DOs Drug Loading, Encapsulation Efficiency and Cumulative Drug Release Rate

The content of pioglitazone in the ultrafiltrate was detected by ultraviolet spectrophotometry, and the mass of free pioglitazone was calculated by comparison to the established linear equation. (Figure 3b) Then, the encapsulation efficiency (EE) and drug loading efficiency (DL) of pioglitazone in the Pio@C-HA-DOs were calculated according to the appropriate formula (Figure 3c). Within a certain range, the encapsulation efficiency increased with a decrease in the ratio of pioglitazone to C-HA-DOs (58.04% to 97.25%). Correspondingly, the drug loading rate decreased from 36.72% to 3.49%. In general, the encapsulation efficiency of micelles needs to be greater than 80% to avoid wasting a large amount of free drug. Combined with the experimental results, a binding ratio of drug to micelles was 1:10 was adopted. Under this condition, the encapsulation efficiency reached a considerable 97.25%, and the drug loading rate was 9.069%. Notably, the encapsulation efficiency of the micelle particles in the 1:25 formulation was not higher than that in the 1:10 formulation, reaching only 89.51%. These data indicated that formulations with a radio of 1:10 and below, the amount of pioglitazone delivered exceeded the capacity of the micelle in solution, and most of the excess drug existed in the free form outside the micelle, thereby reducing the encapsulation efficiency.

The release experiment was performed with PBS solutions at two pH values in a constant temperature incubator at 37°C to simulate the release behaviour of pioglitazone from Pio@C-HA-DOs in the microenvironment surrounding glycosaminoglycans in synovial fluid and cartilage under human physiological conditions (Figure 3d). In pH 7.4 PBS, only 40% of the drug was released from the micelles after 24 hours, which was followed by a steady and slow release for at least 3 days. These data indicated that drug release from the Pio@C-HA-DOs was slow after injection of the micelles into the joint cavity and free from the joint fluid. Pioglitazone release in PBS at pH 6.4 reached 50% at 4 hours, 65% at 12 hours, and 75% to 80% at 24 hours, which means that a lower pH results in faster drug release. There are many factors for rapid drug release in this environment that are different from physiological conditions. First, the size of the micelle particles in the two pH environments is different. Second, the solubility of pioglitazone in water is affected by the pH values. Pioglitazone does not dissolve well in deionized water but easily dissolves in acid. The weak acidification of the solution improved the solubility of pioglitazone and increased the amount of pioglitazone in its free form per unit time. Contrary to expectations, the Pio@C-HA-DO concentration did not affect drug release within a certain range. There was no significant difference in drug release between 1 g/L and 2 times the equivalent number of drug-loaded micelles, and the two micelles displayed almost the same behaviour in PBS at pH 7.4. However, the cumulative drug release from 2 g/L drug-loaded micelles at 24 hours in the lower pH environment was below that from 1 g/L Pio@C-HA-DOs. These results indicated that although increasing the micelle concentration increased the drug release rate per unit of time, it decreased the long-term cumulative drug release rate, which might be limited by the solubility of the drug in solution.

Utilizing a pH-responsive mechanism to control the particle size of the vector and drug release is a well-established approach in drug delivery for the treatment of OA.[42] When considering the acidic microenvironment of and the cartilage layer and articular cartilage glycosaminoglycans in OA, the cartilage glycosaminoglycan sugar chains and inflammation cause the size of the nanomaterial to increase, result in unstable and rapid drug release. The pH-responsiveness of C-HA-DOs and Pio@C-HA-DOs are consistent with other studies.[43–45]

Cytocompatibility of C-HA-DOs and Other Cell Activity Experiments

When synthetic C-HA-DOs are used for intra-articular injection in the treatment of OA, it is first necessary to consider whether they will have toxic effects on chondrocytes. When the concentration of C-HA-DOs ranged from 3 mg/L to 1 g/L, the viability of the chondrocytes co-incubated with the micelles for 24 or 48 hours showed no significant difference compared with the control group ($n \geq 3$). However, when the micelle concentration increased to 3 g/L, the toxicity to the chondrocytes became obvious and further increased with time (Figure 3e). These results suggest that C-HA-DOs have low toxicity to chondrocytes at appropriate concentrations (≤1 g/L) and can be used as a drug carrier for intra-articular injection.

H_2O_2 can induce a model of OA in chondrocytes.[46] Low concentrations of H_2O_2 (< 300 μmol/L) did not cause significant damage to chondrocytes, and when the H_2O_2 concentration reached 400 μmol/L, half of the chondrocytes died after 24 hours (Figure 3f). In subsequent experiments, 400 μmol/L H_2O_2 was used to induce OA.

HA has been shown in previous studies to slow the killing effect of H_2O_2 on chondrocytes.[47] Thus, we tested whether the synthesized C-HA-DOs had the same ability to interfere with H_2O_2. The results showed that HA itself could prevent damage to chondrocytes caused by H_2O_2. As reported in a previous article, a low concentration of C-HA-DOs (0.1 mol/L) could produce more than 70% recovery, while the high concentration of C-HA-DOs allowed almost no effects from H_2O_2 to be observed. This may be related to the rapid removal of reactive oxygen species (ROS) in the environment with HA. C-HA-DOs also had a therapeutic effect in a concentration-dependent manner, but the effect of the C-HA-DOs against H_2O_2 was weaker than that of HA, probably because the modification from the synthesis reaction affected the functional antioxidant domain of HA (Figure 3g).

Effect of C-HA-DOs on ROS in Chondrocytes in the H_2O_2-Induced Model

ROS include superoxide, peroxides, hydroxyl radicals and other chemicals. Under environmental stress, the ROS levels in cells increase sharply, which is called oxidative stress. Therefore, detection of the ROS content in chondrocytes can indirectly reflect their oxidative stress status. The ROS content in chondrocytes in each group was determined by fluorescence microscopy. Green fluorescence represents the DCF generated by reaction of the fluorescent probe DCFH-DA in the ROS kit, and the green fluorescence intensity is proportional to the intracellular ROS level. After the addition of the H_2O_2 modelling agent, the intracellular ROS level increased sharply. Notably, the ROS levels in the chondrocytes treated with C-HA-DOs and Pio@C-HA-DOs returned to close to that in the control, and the inhibitory effect of Pio@C-HA-DOs on ROS was more obvious (Figure 4a and b).

Effect of C-HA-DOs on the Mitochondrial Membrane Potential of Chondrocytes

Maintaining mitochondrial membrane potential homeostasis is the basis of oxidative phosphorylation in chondrocytes. In osteoarthritis model chondrocytes, the mitochondrial membrane potential showed a downwards trend. Once the mitochondrial membrane potential decreases, the cells are on the verge of entering a stage of irreversible apoptosis. JC-1 is a fluorescent probe that can detect the mitochondrial membrane potential ($\Delta\Psi m$). When JC-1 is taken up by normal cells, it can form a polymer and produce red fluorescence, while it exists as a monomer in early apoptotic cells and emits green fluorescence. The ratio of red to green fluorescence can be used to judge the relative degree of apoptosis.

The red fluorescence in Group R was slightly weakened, indicating that the mitochondria in these cells were in a state of suboptimal health. After treatment, the ratio of red to green fluorescence intensity was plotted on the vertical axis. Groups P1 and P2 were treated with the C-HA-DOs and Pio@C-HA-DOs, respectively. H_2O_2 treatment affected the activity of chondrocytes but also reduced the mitochondrial membrane potential of the remaining viable cells, while C-HA-DOs rescued the mitochondrial membrane potential. The recovery of the mitochondrial membrane potential in Group P1 was more complete than that in Group R (Figure 4c and d).

Effect of Oxidative Stress on the Cellular Uptake of C-HA-DOs by Chondrocytes

The uptake of C-HA-DOs by chondrocytes under oxidative stress and normal physiological conditions was evaluated by observing the distribution of Cy5-CHA-DOs in chondrocytes. The uptake of Cy5-C-HA-DOs by chondrocytes under physiological conditions was time dependent, as the amount of Cy5-C-HA-DOs in chondrocytes at 4 hours was nearly

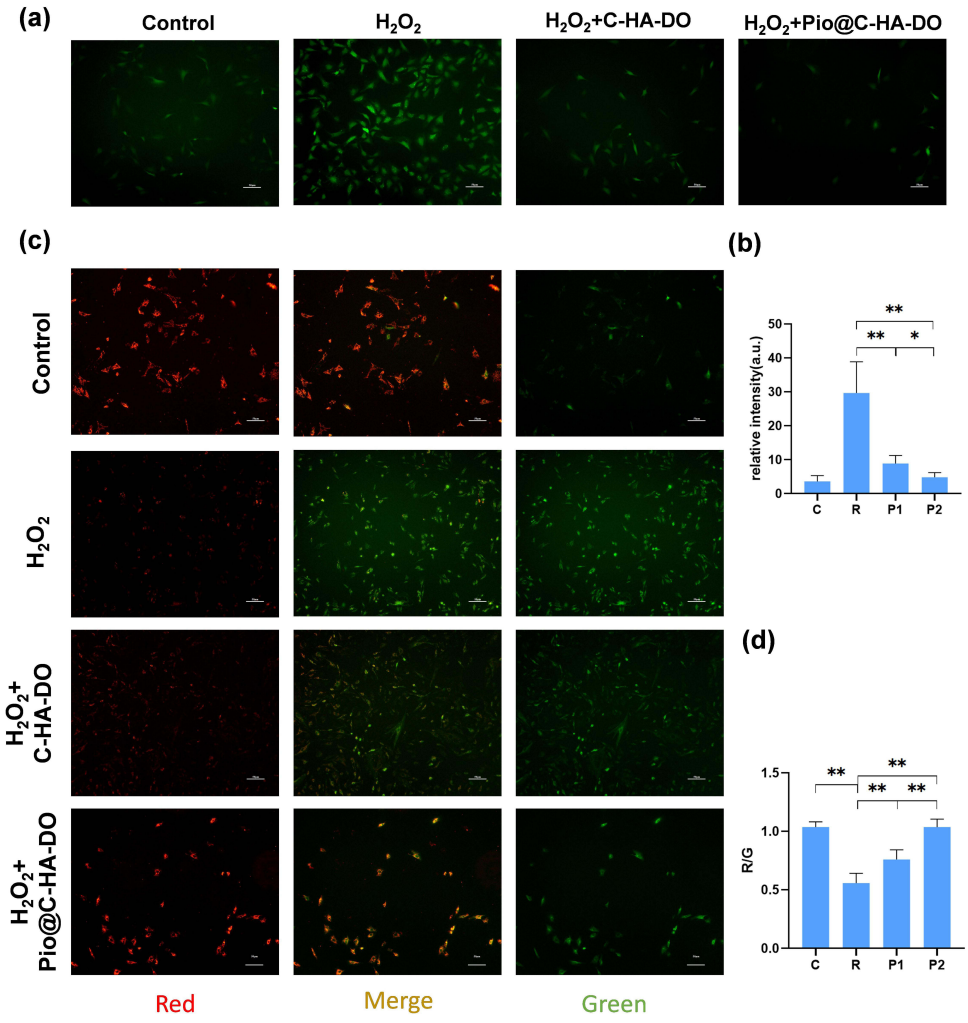

Figure 4 Images of ROS (**a** and **b**) and mitochondrial membrane potential (**c** and **d**) in chondrocytes (100x).
Note: *P<0.05, **P<0.01.
Abbreviations: C, C=control, control group; R, R=H_2O_2, group with 400 μmol/L H_2O_2; P1, P1=(H_2O_2+C-HA-DO), group with 400 μmol/L H_2O_2 and 1 g/L cartilage-targeted hyaluronic acid nano micelles; P2, P2=(H_2O_2+Pio@C-HA-DO), group with 400 μmol/L H_2O_2 and 1 g/L cartilage-targeted hyaluronic acid nano micelles loaded with pioglitazone; ROS, reactive oxygen species; JC-1, mitochondrial membrane potential fluorescent probe; R/G, ratio of red fluorescence intensity to green fluorescence intensity.

twice that at 1 hour. Moreover, the uptake of Cy5-C-HA-DOs by chondrocytes under oxidative stress was faster, and maximum uptake was reached at 1 hour, and this concentration was maintained 4 hours. (Figure 5a and b) The reasons for the faster uptake of Cy5-C-HA-DOs by chondrocytes under oxidative stress may include the following. (a) Chondrocytes under oxidative stress are in a sub healthy state, and their cell membrane permeability is increased, which makes it easier for C-HA-DOs nanoparticles to enter the cells.[48] (b) It has been found that CD44 may be involved in the inflammatory signalling pathway of chondrocytes, and the expression of CD44 increases when chondrocytes are exposed to oxidative stress.[49] Many studies have found that HA can specifically bind to CD44, and HA and CD44 cooperate to promote the cellular uptake of C-HA-DOs by chondrocytes.[50,51]

Effects of H_2O_2, C-HA-DOs, and Pio@C-HA-DOs on OA-Related Gene Expression

Amongst the various genes expressed in OA, here, we focused on type II collagen and aggrecan in chondrocytes as well as the corresponding metalloenzymes that degrade them, as these factors are all closely related to cartilage matrix damage and regenerative repair.[52]

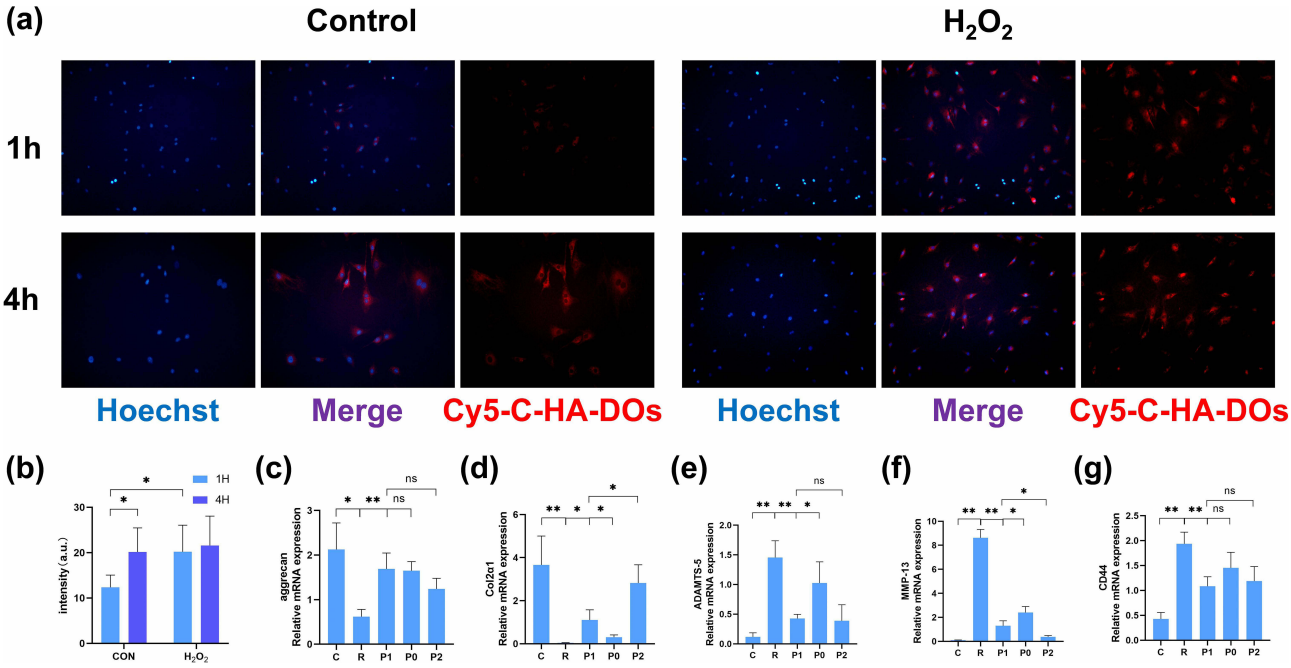

Figure 5 Cellular uptake of Cy5-C-HA-DOs (**a** and **b**) and expression of OA related genes (**c**–**g**).
Notes: *P<0.05, **P<0.01, ns, not significant.
Abbreviations: C, control Group; R, R=H_2O_2, group with 400 μmol/L H_2O_2; P0, P0=(H_2O_2+HA), group with 400 μmol/L H_2O_2 and 1 g/L Hyaluronic acid (5000 Da); P1, P1=(H_2O_2+C-HA-DO), group with 400 μmol/L H_2O_2 and 1 g/L cartilage-targeted hyaluronic acid nano micelles; P2, P2=(H_2O_2+Pio@C-HA-DO), group with 400 μmol/L H_2O_2 and 1 g/L cartilage-targeted hyaluronic acid nano micelles.

We found that H_2O_2 reduced the expression of aggrecan (Figure 5c) and Col2α1 (Figure 5d) in chondrocytes, and which was inhibited by C-HA-DOs. However, there was no significant difference in aggrecan expression in the HA, C-HA-DO and Pio@C-HA-DO groups. Moreover, there were significant differences between the C-HA-DO and HA groups, and between the Pio@C-HA-DO and C-HA-DO groups in term of col2α1 expression. H_2O_2 increased the expression of ADAMTS-5 (Figure 5e) and MMP-13 (Figure 5f) in chondrocytes, which was effectively inhibited by C-HA-DOs. The inhibitory effect of C-HA-DOs was better than that of HA, but only the cells treated with Pio@C-HA-DOs showed better inhibition of MMP-13.

We observed that the expression of CD44 increased when chondrocytes were treated with H_2O_2 (Figure 5g), but HA and C-HA-DOs inhibited this phenomenon to the same extent as Pio@C-HA-DOs. Previous studies have found that CD44 may regulate the expression of catabolic genes, including MMP and ADAMTS, through the NF-κB signalling pathway.[53,54] We considered that C-HA-DOs may affect the expression of a series of genes involved in OA by inhibiting CD44 expression through a similar mechanism.

Histological Observations and OARSI Scores from in vivo Experiments

The gross images show that the articular surfaces in Group C were smooth without osteophyte proliferation or fibrous tissue infiltration. In Group R, the medial cartilage of the tibial plateau was rough and uneven, the synovial membrane and osteophytes around the medial tibial plateau displayed extreme proliferation, and the lateral tibial plateau was worn. In Group P1, the cartilage on the tibial plateau was slightly reduced and there was no obvious wear on the lateral tibial plateau. The wear of the tibial plateau in Group P2 was lighter than that in Group R, the cartilage on the medial tibial plateau was significantly reduced, and the lateral tibial plateau was smooth without cartilage formation (Figure 6a, Gross image).

Haematoxylin-eosin (HE) staining images showed that the surface of the cartilage layer in Group C was flat, the overall morphology of the cartilage was complete, and the cell arrangement was normal. In Group R, the cartilage structure was extensively damaged, the cleft portion penetrated the subchondral bone, there were few chondrocytes, the

fibrous tissue was outside the damaged cartilage layer, and a pannus had formed. In Group P1, the cartilage matrix was relatively abundant, the cartilage layer was relatively complete, the surface was infiltrated by fibrous tissue, the deep layer of chondrocytes was normal, and the surface layer of chondrocytes was disordered. In Group P2, the cartilage surface was relatively smooth and intact, the chondrocytes were arranged normally, and there was no pannus hyperplasia (Figure 6a, HE).

In the Safranin O fast green staining images of Group C, matrix staining was abundant, the surface of the cartilage layer was smooth, the tide line was complete, and the chondrocytes were arranged normally. In Group R, staining of only fibrous tissue and subchondral bone was observed. The extracellular matrix in Group P1 recovered well, and the surface hyaline cartilage structure was disordered. In Group P2, cartilage matrix staining was almost normal, and the hyaline cartilage and fibrocartilage structures were clear (Figure 6a, Safranin O fast green).

Histopathological examinations were performed, and the OARSI score was utilized (Figure 6b). The OARSI score of Group P1 was significantly lower than that of Group R, while the OARSI score of Group P2 was significantly lower than those of Group P1 and Group R. The main reason for this result is that the cartilage layer of Group R was seriously damaged, while in Group P1, a disordered cell arrangement and fibrous tissue proliferation were noted, indicating that C-HA-DOs can alleviate cartilage wear and degradation in OA. This is particularly true when combined with cartilage, which increases the overall staining thickness of the cartilage layer. However, for the cartilage in the cartilage layer, the health status of the cells was not good, although the release of pioglitazone from the cartilage layer effectively improved the health status of the chondrocytes and contributed to the formation of a normal cartilage layer.

Immunohistochemistry

The results of collagen type II immunohistochemical staining showed that the rate of positive collagen type II staining in Group R was lower than that in Group C due to the loss of the cartilage layer, while the rates of positive collagen type II staining in Groups P1 and P2 were higher than that in Group R, and the positive rate in Group P2 was higher than that in Group P1 (Figure 7, Coll-II).

The results of proteoglycan immunohistochemical staining showed that the rate of positive proteoglycan staining in Group R was significantly lower than that in Group C, but there was no significant difference between Groups P1 and R after treatment; only the positive rate between Groups P2 and R differed significantly (Figure 7, Aggrecan).

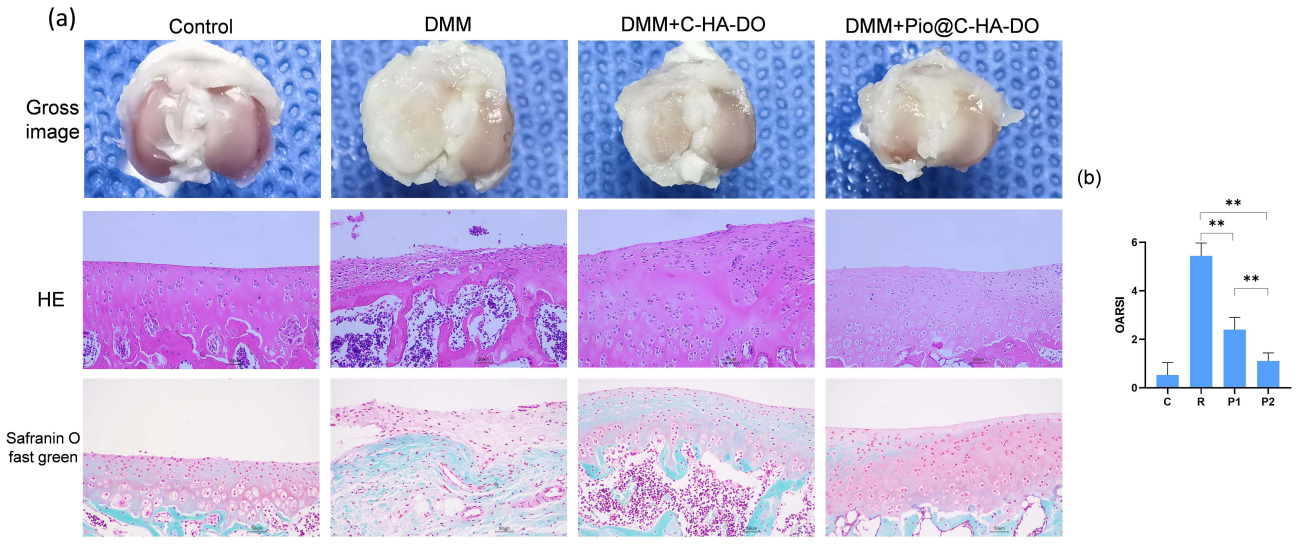

Figure 6 (**a**) Gross, HE staining and safranin O fast green staining images (20x). (**b**) OARSI scores of pathological sections of the tibial plateau of the right knee joint.
Note: **P<0.01, (n≥3).
Abbreviations: C, C=control, sham operation group; R, R= DMM, surgical destabilization of the medial meniscus group; P1, P1= (DMM +C-HA-DO), surgical destabilization of the medial meniscus and articular injection of cartilage-targeted hyaluronic acid nano micelles; P2, P2= (DMM +Pio@C-HA-DO), surgical destabilization of the medial meniscus and articular injection of cartilage-targeted hyaluronic acid nano micelles loaded with pioglitazone; HE, haematoxylin-eosin staining.

Immunohistochemical staining of MMP-13 showed that the expression of the MMP-13 protein in Group R was significantly higher than that in the other groups. The expression of MMP-13 decreased in Groups P1 and P2, and the decrease in Group P2 was more significant (Figure 7, MMP-13).

Immunohistochemical staining of ADAMTS-4 showed that ADAMTS-4 was highly expressed in the lacunae of the chondrocytes and on the surface wear area of the cartilage layer in Group R. There was no significant difference in the positive rate between Groups P1 and R, and only the positive rate between Groups P2 and R differed significantly (Figure 7, ADAMTS-4).

Collagen type II, proteoglycan, ADAMTS-4, and MMP-13 are important indicators of OA, amongst which ADAMTS-4 is one of the metalloenzymes that degrades proteoglycan, and MMP-13 is one of the metalloenzymes that degrades collagen. Thus, the corresponding expression index can reflect the health of the osteoarthritic cartilage.[55,56]

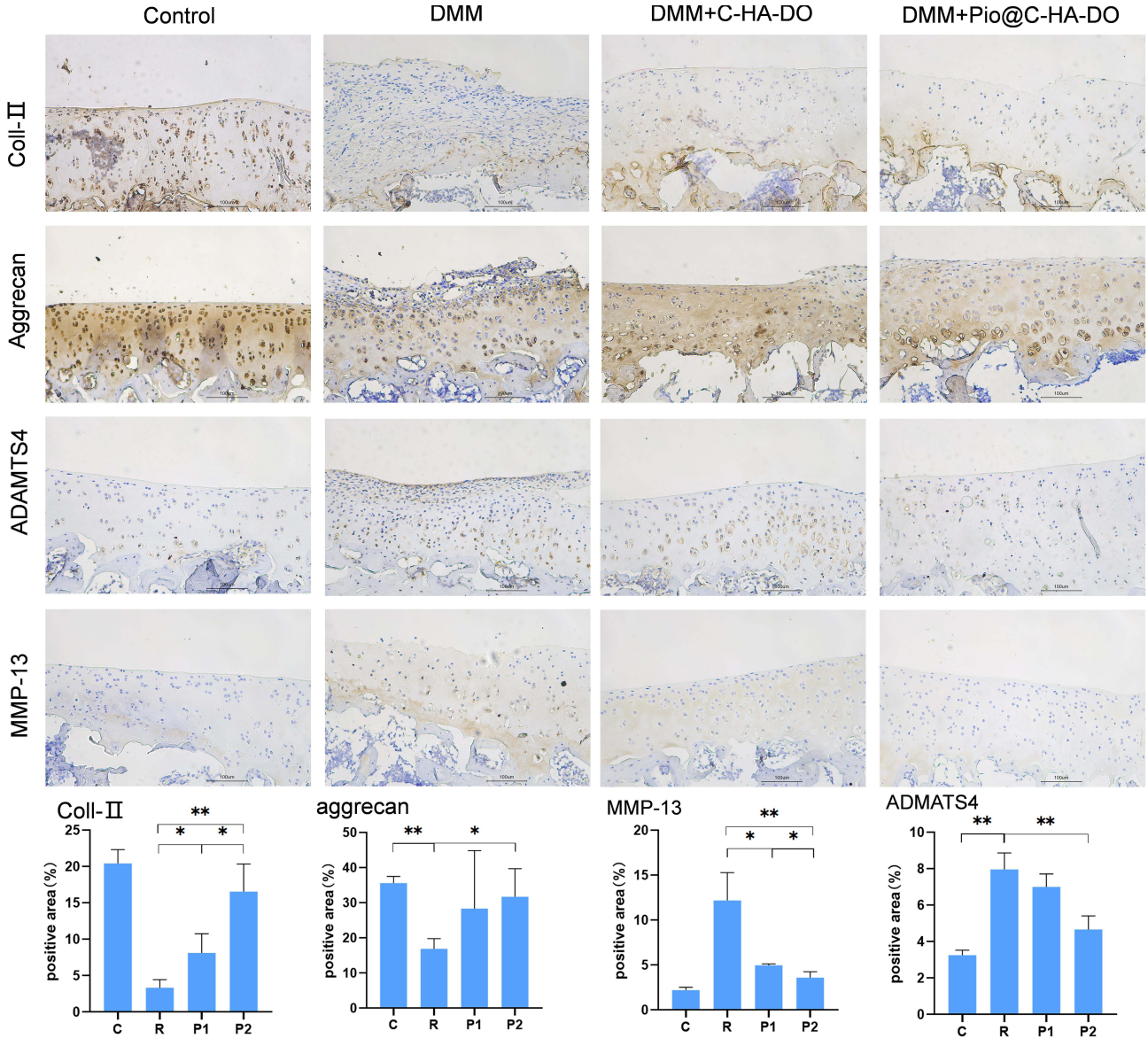

Figure 7 Immunohistochemical staining images and statistical results (40x).
Note: *P<0.05, **P<0.01, n=3.
Abbreviations: C, C=control, sham operation group; R, R= DMM, surgical destabilization of the medial meniscus group; P1, P1=(DMM +C-HA-DO), surgical destabilization of the medial meniscus and articular injection of cartilage-targeted hyaluronic acid nano micelles; P2, P2=(DMM +Pio@C-HA-DO), surgical destabilization of the medial meniscus and articular injection of cartilage-targeted hyaluronic acid nano micelles loaded with pioglitazone; Coll-II, Collagen type II; MMP, Matrix Metalloproteinase; ADAMTS, a disintegrin and metalloproteinase with thrombospondin motifs.

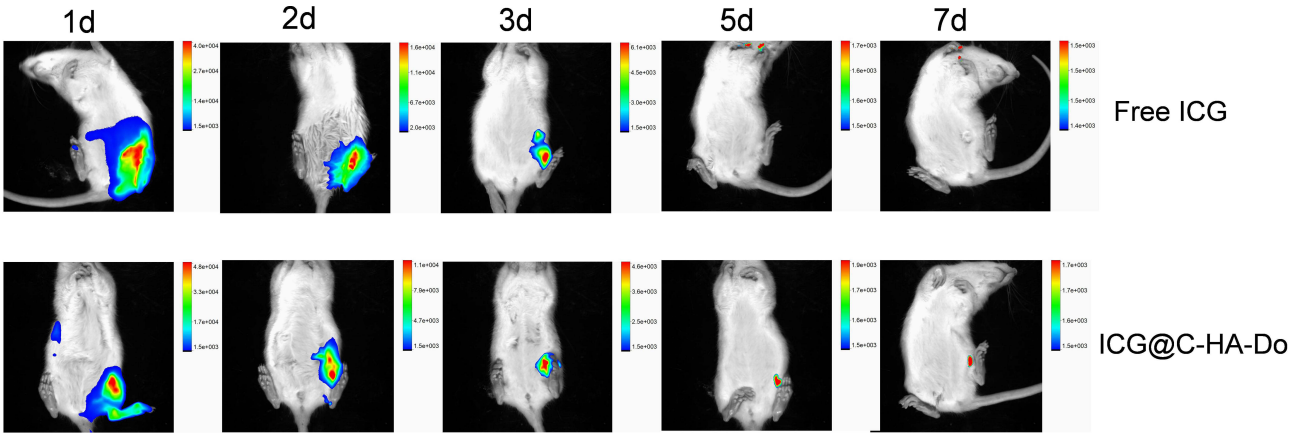

Figure 8 IVIS images.
Notes: MIX=1500 a.u. animals were injected after 1, 2, 3, 5, and 7 days.
Abbreviations: ICG, indocyanine Green; ICG@C-HA-Do, cartilage-targeted hyaluronic acid nano micelles loaded with indocyanine green; IVIS, in vivo small animal fluorescence imaging.

The immunohistochemical results of the tibial plateau sections of the right knees of the rats 6 weeks after modelling showed that the expression of collagen type II and Aggrecan, which are indicators of cartilage health, decreased in the model group. Of note the expression of the corresponding degradation enzymes MMP-13 and ADAMTS-4 increased, which is consistent with reports of OA in the literature.[57]

In both treatment groups, the expression of collagen type II could be restored and that of MMP-13 could be inhibited, but only the group loaded with pioglitazone could slow the degradation of Aggrecan by inhibiting the expression of ADAMTS-4, indicating that C-HA-DOs themselves can inhibit MMP-13 to delay OA. However, Pio@C-HA-DOs had a better effect, as they can inhibit ADAMTS-4 to prevent OA.

IVIS Imagines

In vivo fluorescence imaging was performed on SD rats at different times after intra-articular injection of ICG. The fluorescence images overlapped with the white light images, and the background was subtracted from the fluorescence results. In the knee joints of rats injected with free ICG, the dispersion of ICG was extensive. Because of its good fluidity, ICG permeated a large area in the surrounding tissues, and it was almost completely cleared from the joint cavity after 5 days (Figure 8). However, when C-HA-DOs were labelled with ICG, the fluorescence was confined to the articular cartilage and did not spread for 7 days. These results indicated that C-HA-DOs were partially bound to the cartilage, which prevented their rapid removal from the joint cavity.

Conclusion

In this study, HA polymer particles with a cartilage-targeting function were synthesized, and their structure was characterized by FT-IR and ^{1}H NMR. The properties of the micelle particles were characterized by a Zetasizer, fluorescence spectrophotometer and transmission electron microscope. Pioglitazone was effectively encapsulated in an appropriate proportion and controlled drug release was achieved under the appropriate pH conditions. In vitro studies showed that the C-HA-DOs have good cytocompatibility at a concentration of 1 g/L and could be efficiently taken up by chondrocytes. C-HA-DOs and Pio@C-HA-DOs inhibited H_2O_2-induced chondrocyte death possibly by reducing the intracellular ROS level or mitochondrial membrane potential, with the effects of Pio@C-HA-DOs being more significant. C-HA-DOs can be rapidly taken up by chondrocytes and inhibit the expression of CD44 and OA-related genes under oxidative stress. Both drug-free C-HA-DOs and Pio@C-HA-DOs improved the osteoarticular cartilage in the in vivo model. Additionally, the C-HA-DOs themselves inhibited the degradation of collagen type II by inhibiting the expression of MMP-13, while pioglitazone inhibited the expression of ADAMTS-4 to ultimately reduce the degradation of Aggrecan in the cartilage matrix to delay the progression of OA.

Acknowledgments

The authors would like to thank Huiqun Hu, Drs, for measuring the size and zeta potential of the micelles, and Mr Weicong Zhu and Mr Yingliang Liu for the guidance with chemical synthesis and analysis.

Funding

This work was financially supported by the Guangdong Provincial Natural Science Foundation [grant number 2019A1515011085] to S.L. and Science and Technology Program of Guangzhou [grant number 202102080344] to Q.M.

Disclosure

The authors report no conflicts of interest in this work.

References

1. Xia B, Di C, Zhang J, Hu S, Jin H, Tong P. Osteoarthritis pathogenesis: a review of molecular mechanisms. *Calcif Tissue Int*. 2014;95(6):495–505. doi:10.1007/s00223-014-9917-9
2. Szilagyi IA, Waarsing JH, Schiphof D, van Meurs JBJ, Bierma-Zeinstra SMA. Towards sex-specific osteoarthritis risk models: evaluation of risk factors for knee osteoarthritis in males and females. *Rheumatology*. 2022;61(2):648–657. doi:10.1093/rheumatology/keab378
3. Ummarino A, Gambaro FM, Kon E, Torres Andón F. Therapeutic manipulation of macrophages using nanotechnological approaches for the treatment of osteoarthritis. *Nanomaterials*. 2020;10(8):1562. doi:10.3390/nano10081562
4. Vina ER, Kwoh CK. Epidemiology of osteoarthritis: literature update. *Curr Opin Rheumatol*. 2018;30(2):160–167. doi:10.1097/BOR.0000000000000479
5. Liu K, Cai F, Liu Y, Abulaiti A, Ren P, Yusufu A. Risk factors of ankle osteoarthritis in the treatment of critical bone defects using ilizarov technique. *BMC Musculoskelet Disord*. 2021;22(1):339. doi:10.1186/s12891-021-04214-8
6. Antoni M, Ginot G, Mereb T, et al. Post-traumatic elbow osteoarthritis after radial head arthroplasty: prevalence and risk factors. *Orthop Traumatol Surg Res*. 2021;107(2):102814. doi:10.1016/j.otsr.2021.102814
7. Abramoff B, Caldera FE. Osteoarthritis: pathology, diagnosis, and treatment options. *Med Clin North Am*. 2020;104(2):293–311. doi:10.1016/j.mcna.2019.10.007
8. Wernecke C, Braun HJ, Dragoo JL. The effect of intra-articular corticosteroids on articular cartilage: a systematic review. *Orthop J Sports Med*. 2015;3(5):2325967115581163. doi:10.1177/2325967115581163
9. Patil P, Nene S, Shah S, Singh SB, Srivastava S. Exploration of novel drug delivery systems in topical management of osteoarthritis. *Drug Deliv Transl Res*. 2023;13(2):531–546. doi:10.1007/s13346-022-01229-z
10. Brown S, Kumar S, Sharma B. Intra-articular targeting of nanomaterials for the treatment of osteoarthritis. *Acta Biomater*. 2019;93:239–257. doi:10.1016/j.actbio.2019.03.010
11. Zhang T, Tian T, Zhou R, et al. Design, fabrication and applications of tetrahedral DNA nanostructure-based multifunctional complexes in drug delivery and biomedical treatment. *Nat Protoc*. 2020;15(8):2728–2757. doi:10.1038/s41596-020-0355-z
12. Ma W, Yang Y, Zhu J, et al. Biomimetic nanoerythrosome-coated aptamer-DNA tetrahedron/maytansine conjugates: pH-responsive and targeted cytotoxicity for HER2-positive breast cancer. *Adv Mater*. 2022;34(46):e2109609. doi:10.1002/adma.202109609
13. Zhang T, Tian T, Lin Y. Functionalizing framework nucleic-acid-based nanostructures for biomedical application. *Adv Mater*. 2022;34(46):e2107820. doi:10.1002/adma.202107820
14. Wang Y, Li Y, Gao S, Yu X, Chen Y, Lin Y. Tetrahedral framework nucleic acids can alleviate taurocholate-induced severe acute pancreatitis and its subsequent multiorgan injury in mice. *Nano Lett*. 2022;22(4):1759–1768. doi:10.1021/acs.nanolett.1c05003
15. Zhang M, Zhang X, Tian T, et al. Anti-inflammatory activity of curcumin-loaded tetrahedral framework nucleic acids on acute gouty arthritis. *Bioact Mater*. 2021;8:368–380. doi:10.1016/j.bioactmat.2021.06.003.
16. Li S, Liu Y, Tian T, et al. Bioswitchable delivery of microRNA by framework nucleic acids: application to bone regeneration. *Small*. 2021;17(47):e2104359. doi:10.1002/smll.202104359
17. Qin X, Xiao L, Li N, et al. Tetrahedral framework nucleic acids-based delivery of microRNA-155 inhibits choroidal neovascularization by regulating the polarization of macrophages. *Bioact Mater*. 2021;14:134–144. doi:10.1016/j.bioactmat.2021.11.031
18. Zhou M, Zhang T, Zhang B, et al. A DNA nanostructure-based neuroprotectant against neuronal apoptosis via inhibiting toll-like receptor 2 signaling pathway in acute ischemic stroke. *ACS Nano*. 2022;16(1):1456–1470. doi:10.1021/acsnano.1c09626
19. Zhu J, Yang Y, Ma W, et al. Antiepilepticus effects of tetrahedral framework nucleic acid via inhibition of gliosis-induced downregulation of glutamine synthetase and increased AMPAR internalization in the postsynaptic membrane. *Nano Lett*. 2022;22(6):2381–2390. doi:10.1021/acs.nanolett.2c00025
20. Chen YJ, Chan DC, Lan KC, et al. PPARγ is involved in the hyperglycemia-induced inflammatory responses and collagen degradation in human chondrocytes and diabetic mouse cartilages. *J Orthop Res*. 2015;33(3):373–381. doi:10.1002/jor.22770
21. Chen YJ, Sheu ML, Tsai KS, Yang RS, Liu SH. Advanced glycation end products induce peroxisome proliferator-activated receptor γ down-regulation-related inflammatory signals in human chondrocytes via toll-like receptor-4 and receptor for advanced glycation end products. *PLoS One*. 2013;8(6):e66611. doi:10.1371/journal.pone.0066611
22. Huang H, Wang ZJ, Zhang HB, et al. The function of PPARγ/AMPK/SIRT-1 pathway in inflammatory response of human articular chondrocytes stimulated by advanced glycation end products. *Biol Pharm Bull*. 2019;42(8):1303–1309. doi:10.1248/bpb.b19-00036
23. Ma C, Zhang Y, Li YQ, Chen C, Cai W, Zeng YL. The role of PPARγ in advanced glycation end products-induced inflammatory response in human chondrocytes. *PLoS One*. 2015;10(5):e0125776. doi:10.1371/journal.pone.0125776

24. Li Y, Zhang Y, Chen C, Zhang H, Ma C, Xia Y. Establishment of a rabbit model to study the influence of advanced glycation end products accumulation on osteoarthritis and the protective effect of pioglitazone. *Osteoarthritis Cartilage*. 2016;24(2):307–314. doi:10.1016/j.joca.2015.08.001
25. Chen C, Ma C, Zhang Y, Zeng Y, Li Y, Wang W. Pioglitazone inhibits advanced glycation end product-induced TNF-α and MMP-13 expression via the antagonism of NF-κB activation in chondrocytes. *Pharmacology*. 2014;94(5–6):265–272. doi:10.1159/000369074
26. Wang ZJ, Zhang HB, Chen C, Huang H, Liang JX. Effect of PPARG on AGEs-induced AKT/MTOR signaling-associated human chondrocytes autophagy. *Cell Biol Int*. 2018;42(7):841–848. doi:10.1002/cbin.10951
27. Ai X, Duan Y, Zhang Q, et al. Cartilage-targeting ultrasmall lipid-polymer hybrid nanoparticles for the prevention of cartilage degradation. *Bioeng Transl Med*. 2020;6(1):e10187. doi:10.1002/btm2.10187
28. Ngadimin KD, Stokes A, Gentile P, Ferreira AM. Biomimetic hydrogels designed for cartilage tissue engineering. *Biomater Sci*. 2021;9(12):4246–4259. doi:10.1039/D0BM01852J
29. Tsanaktsidou E, Kammona O, Kiparissides C. Recent developments in hyaluronic acid-based hydrogels for cartilage tissue engineering applications. *Polymers*. 2022;14(4):839. doi:10.3390/polym14040839
30. Rothenfluh DA, Bermudez H, O'Neil CP, Hubbell JA. Biofunctional polymer nanoparticles for intra-articular targeting and retention in cartilage. *Nat Mater*. 2008;7(3):248–254. doi:10.1038/nmat2116
31. Formica FA, Barreto G, Zenobi-Wong M. Cartilage-targeting dexamethasone prodrugs increase the efficacy of dexamethasone. *J Control Release*. 2019;295:118–129. doi:10.1016/j.jconrel.2018.12.025
32. Jiang T, Kan HM, Rajpura K, Carbone EJ, Li Y, Lo KW. Development of targeted nanoscale drug delivery system for osteoarthritic cartilage tissue. *J Nanosci Nanotechnol*. 2018;18(4):2310–2317. doi:10.1166/jnn.2018.14311
33. Hu HY, Lim NH, Ding-Pfennigdorff D, et al. DOTAM derivatives as active cartilage-targeting drug carriers for the treatment of osteoarthritis. *Bioconjug Chem*. 2015;26(3):383–388. doi:10.1021/bc500557s
34. Gao QQ, Zhang CM, Zhang EX, et al. Zwitterionic pH-responsive hyaluronic acid polymer micelles for delivery of doxorubicin. *Colloids Surf B Biointerfaces*. 2019;178:412–420. doi:10.1016/j.colsurfb.2019.03.007
35. Zhong WZ, Williams MG. Simultaneous quantitation of pioglitazone and its metabolites in human serum by liquid chromatography and solid phase extraction. *J Pharm Biomed Anal*. 1996;14(4):465–473. doi:10.1016/0731-7085(95)01665-1
36. Shakeri F, Shakeri S, Hojjatoleslami M. Preparation and characterization of carvacrol loaded polyhydroxybutyrate nanoparticles by nanoprecipitation and dialysis methods. *J Food Sci*. 2014;79(4):N697–N705. doi:10.1111/1750-3841.12406
37. Xue S, Zhou X, Sang W, et al. Cartilage-targeting peptide-modified dual-drug delivery nanoplatform with NIR laser response for osteoarthritis therapy. *Bioact Mater*. 2021;6(8):2372–2389. doi:10.1016/j.bioactmat.2021.01.017
38. Fang H, Huang L, Welch I, et al. Early changes of articular cartilage and subchondral bone in the DMM mouse model of osteoarthritis. *Sci Rep*. 2018;8(1):2855. doi:10.1038/s41598-018-21184-5
39. Gerwin N, Bendele AM, Glasson S, Carlson CS. The OARSI histopathology initiative - recommendations for histological assessments of osteoarthritis in the rat. *Osteoarthritis Cartilage*. 2010;18(Suppl 3):S24–S34. doi:10.1016/j.joca.2010.05.030
40. D'Este M, Eglin D, Alini M. A systematic analysis of DMTMM vs EDC/NHS for ligation of amines to hyaluronan in water. *Carbohydr Polym*. 2014;108:239–246. doi:10.1016/j.carbpol.2014.02.070
41. Bajpayee AG, Grodzinsky AJ. Cartilage-targeting drug delivery: can electrostatic interactions help? *Nat Rev Rheumatol*. 2017;13(3):183–193. doi:10.1038/nrrheum.2016.210
42. Xu XL, Xue Y, Ding JY, et al. Nanodevices for deep cartilage penetration. *Acta Biomater*. 2022;154:23–48. doi:10.1016/j.actbio.2022.10.007
43. Zhang ZJ, Hou YK, Chen MW, et al. A pH-responsive metal-organic framework for the co-delivery of HIF-2α siRNA and curcumin for enhanced therapy of osteoarthritis. *J Nanobiotechnology*. 2023;21(1):18. doi:10.1186/s12951-022-01758-2
44. Wang Z, Zhong Y, He S, et al. Application of the pH-responsive PCL/PEG-nar nanofiber membrane in the treatment of osteoarthritis. *Front Bioeng Biotechnol*. 2022;10:859442. doi:10.3389/fbioe.2022.859442.
45. Zerrillo L, Que I, Vepris O, et al. pH-responsive poly(lactide-co-glycolide) nanoparticles containing near-infrared dye for visualization and hyaluronic acid for treatment of osteoarthritis. *J Control Release*. 2019;309:265–276. doi:10.1016/j.jconrel.2019.07.031
46. Xu K, He Y, Moqbel SAA, Zhou X, Wu L, Bao J. SIRT3 ameliorates osteoarthritis via regulating chondrocyte autophagy and apoptosis through the PI3K/Akt/mTOR pathway. *Int J Biol Macromol*. 2021;175:351–360. doi:10.1016/j.ijbiomac.2021.02.029
47. Li S, Yang X, Feng Z, Wang P, Zhu W, Cui S. Catalase enhances viability of human chondrocytes in culture by reducing reactive oxygen species and counteracting tumor necrosis factor-α-induced apoptosis. *Cell Physiol Biochem*. 2018;49(6):2427–2442. doi:10.1159/000493841
48. Shchulkin AV, Abalenikhina YV, Erokhina PD, Chernykh IV, Yakusheva EN. The role of P-glycoprotein in decreasing cell membranes permeability during oxidative stress. *Biochemistry*. 2021;86(2):197–206. doi:10.1134/S0006297921020085
49. Qadri M, Almadani S, Jay GD, Elsaid KA. Role of CD44 in regulating TLR2 activation of human macrophages and downstream expression of proinflammatory cytokines. *J Immunol*. 2018;200(2):758–767. doi:10.4049/jimmunol.1700713
50. Bayer IS. Hyaluronic acid and controlled release: a review. *Molecules*. 2020;25(11):2649. doi:10.3390/molecules25112649
51. Kang LJ, Yoon J, Rho JG, et al. Self-assembled hyaluronic acid nanoparticles for osteoarthritis treatment. *Biomaterials*. 2021;275:120967. doi:10.1016/j.biomaterials.2021.120967
52. Malemud CJ. MicroRNAs and Osteoarthritis. *Cells*. 2018;7(8):92. doi:10.3390/cells7080092
53. Kataoka Y, Ariyoshi W, Okinaga T, et al. Mechanisms involved in suppression of ADAMTS4 expression in synoviocytes by high molecular weight hyaluronic acid. *Biochem Biophys Res Commun*. 2013;432(4):580–585. doi:10.1016/j.bbrc.2013.02.043
54. Yasuda T. Type II collagen peptide stimulates Akt leading to nuclear factor-κB activation: its inhibition by hyaluronan. *Biomed Res*. 2014;35(3):193–199. doi:10.2220/biomedres.35.193
55. Mongkhon JM, Thach M, Shi Q, Fernandes JC, Fahmi H, Benderdour M. Sorbitol-modified hyaluronic acid reduces oxidative stress, apoptosis and mediators of inflammation and catabolism in human osteoarthritic chondrocytes. *Inflamm Res*. 2014;63(8):691–701. doi:10.1007/s00011-014-0742-4
56. Yang CY, Chanalaris A, Troeberg L. ADAMTS and ADAM metalloproteinases in osteoarthritis - looking beyond the 'usual suspects'. *Osteoarthritis Cartilage*. 2017;25(7):1000–1009. doi:10.1016/j.joca.2017.02.791
57. Hu Q, Ecker M. Overview of MMP-13 as a promising target for the treatment of osteoarthritis. *Int J Mol Sci*. 2021;22(4):1742. doi:10.3390/ijms22041742